

Lawrence Berkeley National Laboratory

LBL Publications

Title

Climate regime shift and forest loss amplify fire in Amazonian forests

Permalink

<https://escholarship.org/uc/item/0qq5t668>

Journal

Global Change Biology, 26(10)

ISSN

1354-1013

Authors

Xu, Xiyan

Jia, Gensuo

Zhang, Xiaoyan

et al.

Publication Date

2020-10-01

DOI

10.1111/gcb.15279

Peer reviewed

Climate regime shift and forest loss amplify fire in Amazonian forests

Running Title: Climate shift and forest loss amplify fire

Xiyan Xu^{1*}, Gensuo Jia^{1*}, Xiaoyan Zhang², William J. Riley³, Ying Xue⁴,

¹Key Laboratory of Regional Climate-Environment for Temperate East Asia, Institute of Atmospheric Physics, Chinese Academy of Sciences, Beijing 100029, China

²School of Atmospheric Science, Nanjing University of Information Science and Technology, Nanjing 210044, China

³Climate and Ecosystem Sciences Division, Lawrence Berkeley National Laboratory, Berkeley, California 94720, USA

⁴School of Applied Meteorology, Nanjing University of Information Science and Technology, Nanjing 210044, China

*Correspondence:

Xiyan Xu, Email: xiyan.xu@tea.ac.cn, Phone: +86-10-82995472

Gensuo Jia, Email: jjong@tea.ac.cn, Phone: +86-10-82995314

1 **Abstract**

2 Frequent Amazonian fires over the last decade have raised the alarm about the fate of
3 the Earth's most biodiverse forest. The increased fire frequency has been attributed to altered
4 hydrological cycles. However, observations over the past few decades have demonstrated
5 hydrological changes that may have opposing impacts on fire, including higher basin-wide
6 precipitation and increased drought frequency and severity. Here, we use multiple satellite
7 observations and climate reanalysis datasets to demonstrate compelling evidence of increased
8 fire susceptibility in response to climate regime shifts across Amazonia. We show that
9 accumulated forest loss since 2000 warmed and dried the lower atmosphere, which reduced
10 moisture recycling and resulted in increased drought extent and severity, and subsequent fire.
11 Extremely dry and wet events accompanied with hot days have been more frequent in
12 Amazonia due to climate shift and forest loss. Simultaneously, intensified water vapor
13 transport from the tropical Pacific and Atlantic increased high-altitude atmospheric humidity
14 and heavy rainfall events, but those events did not alleviate severe and long-lasting droughts.
15 Amazonia fire risk is most significant in the southeastern region where tropical savannas
16 undergo long seasonally dry periods. We also find that fires have been expanding through the
17 wet-dry transition season and northward to savanna-forest transition and tropical seasonal
18 forest regions in response to increased forest loss at the "Arc of Deforestation". Tropical forests,
19 which have adapted to historically moist conditions, are less resilient and easily tip into an
20 alternative state. Our results imply forest conservation and fire protection options to reduce the
21 stress from positive feedback between forest loss, climate change, and fire.

22

23 **Keywords:** Amazonia; Climate shift; Drought; Forest loss; Savanna; Seasonal forest; Fire

24 **1. Introduction**

25 Amazonian forests have been under serious and increasing threats from extensive
26 climate change, deforestation, and fires. The major concern, primarily based on global climate
27 model simulations, is that Amazonia and its surroundings are anticipated to experience warmer
28 and potentially drier climate (Christensen et al., 2013). The resulting climate-induced plant
29 water stress is likely to cause forest canopy dieback and increase fire susceptibility during this
30 century (Malhi et al., 2009). Two opposing hydrological trends that affect fire susceptibility
31 have been observed within recent decades. First, the hydrological cycle has intensified as
32 evidenced from increased Amazon river discharge and basin-wide precipitation in the past
33 several decades (Gloor et al., 2013; Skansi et al., 2013). Second, in contrast, increased drought
34 frequency and severity has been reported (Fu et al., 2013), which enhances forest flammability
35 and suppresses tree growth (Nepstad et al., 2004).

36 Changes in the Amazonian hydrological cycle have been attributed to large scale
37 climate change, deforestation, or their interactions (Trenberth et al., 2014; Zhang et al., 2017).
38 The intensified wet season precipitation in the last three decades coincided with a warming
39 tropical Atlantic that increased atmospheric water vapor transport to Amazonia (Gloor et al.,
40 2013). Strong tropical Atlantic warming and tropical Pacific cooling strengthens the Walker
41 circulation, which causes wet seasons to be wetter and dry seasons to be drier (Barichivich et
42 al., 2018). These results, and others (Espinoza et al., 2019), indicate that the combined impact
43 of the tropical Pacific and Atlantic oceans on Amazonian drought is complex and are linked to
44 phases of the El Niño-Southern Oscillation (ENSO) and the North Atlantic Oscillation (NAO)
45 (Yoon & Zeng, 2010).

46 Changes in hydrological dynamics in Amazonia due to deforestation have been the
47 focus of many studies (e.g., (Cavalcante et al., 2019; Chambers & Artaxo, 2017; D’Almeida et
48 al., 2007; Staal et al., 2020)). About one-third of the moisture that forms precipitation over the

49 Amazonia is locally supplied through recycling of evapotranspiration (Davidson et al., 2012).
50 Deforestation causes a decline in both evapotranspiration from deforested regions and
51 downwind transport of water vapor (Ellison et al., 2017). As a result, deforestation reduces
52 precipitation and increases the amplitude of droughts in the region (Bagley et al., 2013).
53 Extensive deforestation significantly alters river discharge and flood-pulse magnitude (Coe et
54 al., 2009). The loss of vegetation canopy can lead to increased runoff due to reduction in canopy
55 interception and evapotranspiration (Clark, 1987), which increases surface runoff and
56 amplifies flood risk and severity (Bradshaw et al., 2007). Fragmented forests due to
57 deforestation are prone to drought and flood damage, which exacerbates tree mortality and fire
58 vulnerability (Laurance & Williamson, 2001).

59 Risks of fire increase as forests become stressed by climate change and forest loss.
60 Shifted seasonality (Fu et al., 2013) and extreme weather and climate events (Negrón-Juárez
61 et al., 2018; Nepstad et al., 2007) increase tree mortality. Trees are particularly vulnerable to
62 repeated and prolonged droughts (Phillips et al., 2010; Taufik et al., 2017). The process of
63 reducing live canopy fuels and increasing dead fuels influences the spread and intensity of
64 fires (Stephens et al., 2018). Deforestation leads to increases in downed woody debris and
65 therefore greater fuel mass (Uhl & Kauffman, 1990). Furthermore, forest fragments resulting
66 from deforestation and agricultural expansion are fire-prone because they are often adjacent
67 to cattle pastures and are therefore drier and warmer (Laurance et al., 2018) and more often
68 logged and burned (Laurance & Williamson, 2001). Tree mortality due to climate change or
69 deforestation allows sunlight to heat the forest floor and dry out litter fuel, making it more
70 flammable (Messina & Cochrane, 2007).

71 Although climatic and anthropogenic threats facing Amazonian forests have caused
72 great concern among scientific communities, current understanding of linkages between climate
73 change and deforestation-induced hydrological changes and fire susceptibility are isolated and

74 qualitative, based mainly on reviews of individual studies (Cochrane & Barber, 2009; Davidson
75 et al., 2012; Malhi et al., 2008; Nobre et al., 2016). Here we use multiple satellite observations
76 and climate reanalysis datasets to explore spatial and temporal changes in Amazonia fire
77 regime in that experiences seasonal dry period and examine responses to climate regime shifts
78 and forest loss.

79 **2. Data and Methods**

80 **2.1 Climate regime analysis**

81 The Amazonia extends over three tropical climate zones (Supplementary **Figure S1a**):
82 tropical rainforest (Af), tropical monsoon (Am), and tropical winter dry (Aw) climates
83 according to Köppen-Geiger climate classification for 1951-2000 period at 0.5-degree (Beck
84 et al., 2018). Tropical rainforest climate is wet and humid year-round with dominant land cover
85 of tropical rainforest. The tropical monsoon and tropical winter dry climates are characterized
86 by contrasting wet and dry seasons. The dry and wet seasons extend over August-October and
87 January-March, respectively, with other months transitioning between wet-dry and dry-wet
88 seasons. The land cover in the winter dry zone is dominated by tropical savannas. Tropical
89 seasonal forests or monsoon forests, which are in the transitional region between rainforests
90 and savannas, dominate the tropical monsoon zone (Wright et al., 2017).

91 We calculated the 30-year (1961-1990) mean climate of the Am and Aw in the south
92 of Af where Am and Aw share a similar seasonal precipitation pattern, despite precipitation
93 gradient from the northwest to southeast across Am and Aw. Monthly total precipitation was
94 calculated from 0.5-degree Global Precipitation Climatology Centre (GPCC) monthly
95 precipitation dataset (Schneider et al., 2011). Monthly mean temperature was calculated from
96 0.5-degree GHCN_CAMS Gridded 2 m temperature (Fan & van den Dool, 2008). We defined
97 three three-month periods with distinctive precipitation patterns for our analysis: (1) January
98 to March, with the highest precipitation, is the wet season; (2) August to October, with lowest

99 precipitation, is the dry season; and (3) May to July, with gradual increases in precipitation, is
100 the transition season (Supplementary **Figure S1b-e**).

101 The 2 m air temperature, precipitation, column water vapor, vertically integrated water
102 vapor transport, meridional and zonal wind at 850 hpa were analyzed with European Centre
103 for Medium-Range Weather Forecasts (ECMWF) ERA5 monthly reanalysis at 0.25-degree
104 (ERA5, 2019). All variables were resampled to 0.5-degree using 2×2 0.25-degree grids to
105 accommodate the resolution of Köppen-Geiger climate classification. The relative changes of
106 all the variables between two periods, 1981-2000 and 2001-2018, were calculated for Am and
107 Aw. Probability density functions (Weibull distribution) of monthly mean air temperature and
108 monthly total precipitation were analyzed for wet, transition, and dry seasons in 1981-2000
109 and 2001-2018 periods. Changes in 1000 hpa to 500 hpa relative humidity between 2001-2018
110 and 1981-2000 were calculated to quantify the vertical profile of moisture change.

111 Drought conditions in Am and Aw were analyzed with the Self-calibrating Palmer
112 Drought Severity Index (scPDSI) (Barichivich et al., 2019; van der Schrier et al., 2013).
113 scPDSI was calculated from precipitation and temperature time series with fixed parameters
114 related to soil and surface characteristics at each gridcell. Dry and wet conditions were
115 classified into 11 categories (Table S1) as defined by Palmer for the PDSI (Palmer, 1965).
116 scPDSI in this study spanning the period 1981-2018 was calculated using CRU monthly
117 surface climate data version CRU TS4.03 at 0.5-degree. Time series of scPDSI for wet,
118 transition and dry seasons in the entire Am and Aw region were calculated. The probability
119 density functions (kernel distribution) of scPDSI were analyzed for wet, transition, and dry
120 seasons in 1981-2000 and 2001-2018 periods.

121 **2.2 Biophysical impact of forest loss**

122 The global forest change (GFC) dataset (Hansen et al., 2013) at 30-meter resolution,
123 between 2000 and 2017 provides forest cover information in 2000 and forest loss and gain for

124 each year during the period. Forest loss and gain are defined as the transition from forest to
125 non-forest, and non-forest to forest, respectively, by taking forest cover in 2000 as a base
126 condition. We resampled forest cover and forest change to 0.05-degree and calculated the
127 percent of forest cover in 2000 and accumulative forest loss since 2000 in each 0.05-degree
128 grid.

129 We distinguished disturbed forests from pristine forests and compared observationally-
130 derived evapotranspiration and land surface temperatures between them for Am and Aw to
131 explore the impact of forest loss on local temperature and water conditions. Disturbed forest
132 and pristine forests were screened with 0.05-degree grids by a window searching method (Li
133 et al., 2015). Disturbed forests are identified according to the criteria: (a) forest cover (F_{cover})
134 in 2000 was greater than 70% and (b) the accumulated loss (F_{loss}) during 2001-2017 was greater
135 than 65%. Pristine forest is identified according to the criteria (a) F_{cover} in 2000 was greater
136 than 70% and (b) F_{loss} during 2000-2017 was less than 5%. We then searched 10×10 0.05-
137 degree grids within each 0.5-degree gridcell with the assumption that the background climate
138 is similar in each 0.5-degree gridcell. If disturbed and pristine forests were both present in the
139 same 0.5-degree gridcell, this 0.5-degree gridcell is valid for comparison of the land surface
140 temperature, water, and energy fluxes between disturbed and pristine forests to analyze
141 biophysical impacts of forest loss. As a result, 33 gridcells for Am and 183 grids for Aw were
142 used to calculate the biophysical impacts of forest loss.

143 We used Moderate Resolution Imaging Spectroradiometer (MODIS) Aqua 8-day Land
144 Surface Temperature and Emissivity (LST&E) L3 Global products (MYD11C2 Version 6)
145 (Wan, Hook, & Hulley, 2015) to quantify the land surface temperature changes due to forest
146 loss. MYD11C2 is configured on a 0.05-degree latitude/longitude climate modeling grid.

147 MODIS Bidirectional Reflectance Distribution Function and Albedo (BRDF/Albedo)
148 dataset (MCD43C3 Version 6) (Schaaf & Wang, 2015) were used to quantify albedo changes

149 due to forest loss. MCD43C3 is produced daily using 16-day of Terra and Aqua MODIS data
150 in a 0.05-degree Climate Modeling grid. MCD43C3 provides black-sky albedo (directional
151 hemispherical reflectance) and white-sky albedo (bihemispherical reflectance) at local solar
152 noon. Actual clear sky albedo (blue-sky albedo) is calculated as the mean of black-sky and
153 white-sky albedo because of their small differences and high correlation (Li et al., 2015).

154 We used the MODIS evapotranspiration and latent heat flux product (MOD16A2 Version
155 6) (Running et al., 2017) of 8 day temporal resolution and 500 m spatial resolution to quantify
156 evapotranspiration changes due to forest loss. MOD16A2 collection is derived based on the
157 logic of the Penman-Monteith equation by using daily meteorological reanalysis data with
158 MODIS vegetation property dynamics, albedo, and land cover. We resampled MOD16A2 from
159 500 m to 0.05-degree using bilinear interpolation provided by MODIS reprojection tool (MRT).

160 We assume the background climate is similar in each 0.5-degree grid, so that the
161 temperature and energy fluxes difference in disturbed (D) and pristine (P) 0.05-degree grids in
162 the same 0.5-degree grid is caused by the forest loss. The land surface temperature change
163 (ΔLST) due to accumulated forest loss was calculated as the difference of LST in disturbed
164 forest grids (LST_D) and LST in pristine forest grids (LST_P) in 2017,

$$\Delta LST = LST_D - LST_P \quad (1)$$

165 ΔLST was calculated with MODIS Aqua 8-day Land Surface Temperature and
166 Emissivity (LST&E) L3 Global products (MYD11C2 Version 6).

167 The evapotranspiration change (ΔET), latent heat change (ΔLE) and albedo change (Δ
168 *Albedo*) due to accumulated forest change were calculated following the same way as LST,

$$\Delta ET = ET_D - ET_P \quad (2)$$

$$\Delta LE = LE_D - LE_P \quad (3)$$

$$\Delta Albedo = Albedo_D - Albedo_P \quad (4)$$

169 The subscripts D and P denote the disturbed and pristine forest grids, respectively. ΔET and
170 ΔLE were calculated with MODIS evapotranspiration and latent heat flux product (MOD16A2
171 V6). $\Delta Albedo$ was calculated from Equation (4) with MODIS Bidirectional Reflectance
172 Distribution Function and Albedo (BRDF/Albedo) dataset (MCD43C3 V6).

173 The surface shortwave net radiation change ($\Delta SSNR$) between disturbed and pristine
174 forest grids was calculated as,

$$\begin{aligned}\Delta SSNR &= (1 - Albedo_D) \times S_{in} - (1 - Albedo_P) \times S_{in} & (5) \\ &= -\Delta Albedo \times S_{in}\end{aligned}$$

175 where S_{in} is the downward shortwave radiation from CERES EBAF Surface Product. Under
176 clear sky conditions, S_{in} is assumed homogeneously distributed in the 0.5-degree grid.

177 **2.3 Fire regime analysis**

178 We used two burn area (BA) datasets to analyze the spatial and temporal variation of
179 fire burn area within and across the south boundary of Amazon basin. The ESA Fire Climate
180 Change Initiative (Fire CCI) Dataset Collection (Otón et al., 2019) is generated from Advanced
181 Very High Resolution Radiometer (AVHRR) images under the land long term data record
182 (LTDR) project. Fire CCI spans from January, 1982 to December, 2017 with monthly
183 resolution. BA in 1994 was excluded due to data quality issues. The spatial resolution of Fire
184 CCI is 0.05-degree. Global Fire Emissions Database, Version 4.1 (GFEDv4) (Randerson et al.,
185 2018) provides monthly burned area over June, 1995 - December, 2016 of 0.25-degree spatial
186 resolution. We integrated the total burn area in each 0.5-degree for Fire CCI (10×10 0.05-
187 degree) and GFEDv4 (2×2 0.25-degree) to accommodate the spatial resolution of Köppen-
188 Geiger climate classification and other climate reanalysis data. The 1982-2017 annual mean
189 fraction of burned area and monthly mean burned area were plotted with Fire CCI. We used
190 GFEDv4 from January 2001 to December 2016, to compare burned fraction and area with that

191 by Fire CCI. Fire CCI and GFEDv4 showed comparative spatial pattern and burned area during
192 2001-2016 (Table S2).

193 The annual mean burned area (Ba) in 2001-2017 is compared with that in 1982-2001
194 to examine the spatial pattern of burned area change in dry and transition season. The number
195 of gridcell with increased burned area ($\Delta Ba > 0$) and disturbed forest is counted to evaluate the
196 tendency of burning with forest loss. We further classify the forest loss fraction to four levels,
197 i.e., 0-10%, 10-20%, 20-30%, 30-40% and >40% to identify the probability of increased burn
198 area.

199 **3. Results**

200 **3.1 Decadal climate regime shift to intensified climate extremes**

201 In the past four decades, Amazonian climate has experienced abrupt changes. Mean
202 monthly precipitation after 2001 increased by 3.3-14.5% in different seasons and climate zones
203 compared to that during 1981-2000 (**Figure 1a-b**). The increased precipitation coincided with
204 higher total column moisture content, which is consistent with enhanced water vapor transport
205 from the tropical Pacific to the whole basin in the wet season and from the tropical Atlantic to
206 southeastern Amazonia in the transition and dry seasons (**Figure 2**) between 2001 and 2018. In
207 both Am and Aw, enhanced precipitation was mainly in the form of intensified precipitation
208 (**Figure 1c-d**). In Am, low precipitation frequency and rain-free days also increased,
209 particularly in the dry season.

210 The increased frequency of extremely low and high precipitation was accompanied by
211 warming in Am and Aw, with near-surface air temperatures (2-m temperature) rising at about
212 $\sim 0.10^\circ\text{C decade}^{-1}$ and $\sim 0.12^\circ\text{C decade}^{-1}$, respectively. As a result, annual mean air temperature
213 in the recent two decades (2001-2018) was about 0.20°C higher in Aw and 0.24°C higher
214 (increased by 0.90%) in Am, compared to 1981-2000. The warming in both Am and Aw was

215 mainly contributed by increased occurrence of high temperatures in the wet and transition
216 seasons, while in the dry season the warming was mainly due to decreased occurrence of low
217 temperatures (**Figure 1e-f**).

218 The shifted seasonal temperature and precipitation distributions coincided with more
219 extremely dry and wet conditions in Am and Aw despite the increased total precipitation and
220 column water vapor content. The drought severity and extent both increased according to the
221 self-calibrating Palmer Drought Severity Index (scPDSI) (Barichivich et al., 2019; van der
222 Schrier et al., 2013) (**Figure 3**). The regional mean scPDSI over the periods 1999-2004 and
223 2009-2015 indicated sustained drought conditions ($\text{scPDSI} < -0.5$) (**Figure 3a-c**). On average,
224 the areal extent of (1) normal and near-normal drought conditions ($-1 < \text{scPDSI} < 1$) have been
225 decreasing at 2.0-4.8% decade⁻¹ ($p < 0.001$); (2) slight to extremely dry conditions ($\text{scPDSI} <$
226 -1) have been increasing at 1.9-4.9% decade⁻¹ ($p \leq 0.01$); and (3) slightly to extremely wet
227 conditions ($\text{scPDSI} > 1$) have been increasing at 0.7-1.7% decade⁻¹ (insignificant, $0.4 < p < 0.9$)
228 (Supplementary **Figure. S2**). Over the four decades, drought conditions became more severe
229 in dry and transition seasons and extended into wet and transition seasons.

230 Between 1981-2000, the seasonal scPDSI probability distribution function had regular
231 unimodal patterns, i.e., mean water availability in all seasons were near normally distributed
232 with a peak toward being slightly wet ($0.3 < \text{scPDSI} < 0.7$). However, the scPDSI pattern
233 evolved to be more bimodal after 2000, mainly due to increased occurrence of drought. The
234 near-normal condition ($-0.5 < \text{scPDSI} < 0.5$) shifted to more dry conditions ($-2 < \text{scPDSI} <$
235 0.5) in Am, and moderately dry and extremely dry conditions in Aw ($\text{scPDSI} < -2$) (**Figure**
236 **3d-i**). In Aw, droughts in transition and dry seasons expanded to a larger area. Even in the wet
237 season, moderate and extreme droughts increased significantly.

238 **3.2 Warmer and drier lower atmosphere due to forest loss**

239 The Amazonia has experienced intensive forest loss due to deforestation, climate
240 change, and fire. Since the 20th century, reduction in forest cover mainly occurred at “Arc of
241 Deforestation” (Malhi et al., 2008) in eastern and southern Amazonia (**Figure 4a**). The forest
242 loss rates across Af, Am, and Aw have been estimated to be $47.8 \pm 14.9 \text{ } 10^3 \text{ km}^2 \text{ yr}^{-1}$ during
243 2001-2017, in which $11.9 \pm 3.5\%$ of the losses were in tropical rainforest, $23.5 \pm 3.2\%$ in tropical
244 seasonal forest, and $64.6 \pm 5.3\%$ in tropical savannas according to the global forest change
245 dataset.

246 Accumulated forest loss during 2000-2017 resulted in a decline in ET (**Figure 4b-c**).
247 Annual ET decreased by $-76.1 \pm 80.5 \text{ mm y}^{-1}$ and $-213.3 \pm 88.1 \text{ mm y}^{-1}$ for Am and Aw,
248 respectively. The decreased ET occurred across the transition and dry seasons, with maximum
249 decreases in August for Am ($-34.9 \pm 20.1 \text{ mm month}^{-1}$) and Aw ($-36.8 \pm 20.1 \text{ mm month}^{-1}$),
250 respectively. A direct impact of declining ET is reduced atmospheric specific humidity. The
251 observational reanalysis record is consistent with this effect, with the atmosphere drying to an
252 altitude corresponding to 875-850 hpa in transition and dry seasons (**Figure 2d-e**). The near-
253 surface (i.e., below 850 hpa) mean humidity in the transition and dry seasons over 2001-2018
254 decreased by 0.91% and 1.15% for Am and Aw, respectively, relative to 1981-2000.

255 ET requires a substantial amount of energy to vaporize water. ET reductions not only
256 limit water vapor contributions to the lower atmosphere, thereby reducing moisture buffering
257 of temperature changes, but also substantially diminishing surface latent heating. The forest
258 loss caused reductions in annual mean latent heat between 2001-2017 of $-5.9 \pm 6.3 \text{ Wm}^{-2}$ and -
259 $16.6 \pm 6.8 \text{ Wm}^{-2}$ in Am and Aw, respectively. The seasonal pattern of latent heat changes due
260 to forest loss were similar to that of ET, with major reductions in the transition and dry seasons,
261 and maximum reductions in August of $-31.8 \pm 18.4 \text{ Wm}^{-2}$ and $-33.7 \pm 18.4 \text{ Wm}^{-2}$ for Am and Aw,
262 respectively (Supplementary **Figure S3a-b**).

263 The surface warming impacts of reduced latent heating can be partially offset by the
264 cooling impacts of forest loss induced surface albedo change. Accumulated forest loss
265 increased surface albedo in 2001-2017, thereby decreasing annual mean SSNR
266 by $-5.8 \pm 1.7 \text{ W m}^{-2}$ and $-7.2 \pm 1.6 \text{ W m}^{-2}$ for Am and Aw, respectively. This cooling impact is
267 lower in the dry season when the forest canopy is sparser than in the wet season (Supplementary
268 **Figure S3c-d**) and can also be reduced by decreasing cloud cover (and thereby reduced ET
269 (Bala et al., 2007)). The tropical forest loss induced ET and albedo changes and their
270 subsequent cloud and greenhouse gas feedbacks have a net warming impact at the regional
271 scale (**Figure 4d-e**). The accumulated forest loss between 2001-2017 was coincident with an
272 annual mean LST change of $0.9 \pm 0.5^\circ\text{C}$ and $1.2 \pm 0.7^\circ\text{C}$ for Am and Aw, respectively. The
273 warming is most significant in the dry season from August to November.

274 **3.3 Fire expansion due to climate shift and forest loss**

275 The fire burned area across Amazonia is mainly distributed across the southern boundary
276 of the Amazon basin in Am and Aw (**Figure 5a**). Between 1982 and 2017, ~93% of the mean
277 annual burned area occurred in Aw and ~94% of fires occurred in the dry season with peak
278 burn from August to October (**Figure 5b**). Despite interannual variation, the annual total
279 burned area ($178.5 \pm 65.4 \text{ 10}^3 \text{ km}^2$) in Am and Aw was relatively stable between 1982 and 2017.
280 The burned area in Am expanded between 2001 and 2017 relative to between 1982 and 2000.
281 The expanded burn occurred mainly in the transition season between May and August, when
282 the mean fraction of burned area in Am increased from $3.7 \pm 3.7\%$ (1982-2000) to $5.4 \pm 3.4\%$
283 (2001-2017) with a maximum increase in May (about doubling; **Figure 5c**).

284 The disturbed forests in the transition season are more prone to burning than in wet and
285 dry seasons. In the transition season, 72% of Aw and 68% of Am (compared to 53% of Aw
286 and 47% of Am in dry season) disturbed forests showed fire increases during 2001 - 2017,

287 compared to during 1982 - 2000. The burned area increased mainly across the southern
288 boundary of the Amazon basin at “Arc of Deforestation” (Supplementary **Figure S4**). However,
289 the burned area decreased in the southern Aw where the climate is much drier and experienced
290 a more intensive drying trend than in Am and northern Aw. Compared to the dry season,
291 transition season fires clearly expanded within and across the southern boundary of the basin
292 where forests are highly disturbed. The fraction of increased burned area is largely dependent
293 on the fraction of forest loss (**Figure 6**). The increased burn rates are higher in the transition
294 seasons than in the dry seasons, particularly in the seasonal forests. Furthermore, the seasonal
295 forests had obvious increases in fires in response to forest loss, while responses to increased
296 tree losses in savannas were relatively stable.

297 **4. Discussion**

298 The Atlantic Ocean supplies two-thirds of Amazonia precipitation (Davidson et al.,
299 2012). Amazonia wetting in recent decades has been attributed to increasing atmospheric water
300 vapor transport from the warming tropical Atlantic (Gloor et al., 2013). Water vapor transport
301 from the tropical Atlantic to southeastern Amazonia in the transition and dry seasons were
302 enhanced between 2001-2018, which can explain the increased precipitation and moisture in
303 savannas. While in seasonal forests, the increased precipitation and moisture were contributed
304 by enhanced water vapor transport from the tropical Pacific. Enhanced water vapor transport
305 from the tropical Pacific in the wet season is consistent with the basin-wide wetting.

306 Increased precipitation occurred mostly in intensified heavy rainfall events. This shifted
307 precipitation pattern of intensified heavy rainfall events and extremely wet days has been
308 observed since the mid-20th century (Skansi et al., 2013). Our results showed increased low
309 precipitation frequency and rain-free days, and enhanced drought severity and extent,
310 particularly in seasonal forests, indicating polarization between extreme precipitation and
311 water stress. The increased wet and dry extremes exacerbate vulnerability and mortality of

312 vegetation (Hirota et al., 2011). The intensified heavy rainfall events cannot effectively ease or
313 alleviate long lasting drought because most of that rainfall runs off into drainage channels and
314 streams rather than being absorbed into the ground (Trenberth et al., 2014). Further, runoff
315 from heavy rainfall events is enhanced in regions of vegetation loss because of reduced rainfall
316 interception, canopy evapotranspiration, and soil infiltration, amplifying flood risk (Bradshaw
317 et al., 2007; Gentry & Lopez-Parodi, 1980; Lawrence & Vandecar, 2015).

318 In Amazonia, forest moisture and thermal conditions are largely driven by tropical
319 Pacific and Atlantic sea surface temperatures (SST) that fluctuate with the ENSO and NAO
320 phases (Jiménez-Muñoz et al., 2016; Zeng et al., 2008). However, some drought events cannot
321 be fully explained by SST anomalies, e.g., the 2015-2016 unprecedented drought (Erfanian et
322 al., 2017). Our results showed that the decreased ET due to forest loss dries the lower
323 atmosphere and likely amplifies drought severity, particularly in tropical savannas. Savanna
324 soils tend to be porous with more rapid drainage than in tropical seasonal forests (Lloyd et al.,
325 2009). Therefore, even in the wet season, tree loss in savannas reduces ET due to low soil
326 water-holding ability. The large decline in ET implies a substantial reduction in water supply
327 to the lower atmosphere since ET accounts for $\sim 1/3^{\text{rd}}$ of Amazonia rainfall (Staal et al., 2018)
328 and $\sim 90\%$ vapor content in near-surface subcanopy layer (Cochrane & Barber, 2009).

329 The contrasting change of specific humidity in the low- and high-level atmosphere
330 implies differences in water supply mechanisms. Increased humidity at all levels in the wet
331 season and upper atmosphere in the transition and dry seasons are consistent with enhanced
332 precipitation and column water vapor content and are more likely explained by increased
333 water vapor transport from the tropical oceans as we found. The level of decreased specific
334 humidity occurs right below 850 hpa, the level at which a large proportion of moisture is
335 conveyed from oceans (Gimeno et al., 2016). However, the drying lower-level atmosphere is
336 consistent with reduced ET, because ET is the major moisture source in the Amazonian low

337 atmosphere (Cochrane & Barber, 2009), which implies a substantial weakening of
338 atmospheric moisture recycling due to forest loss. The decreased moisture recycling due to
339 forest cover loss can substantially delay the initiation of dry-to-wet season transitions (Wright
340 et al., 2017) and extend the dry season (Agudelo et al., 2019).

341 The spatial gradient of fire from northwest to southeast is related to climate patterns
342 and forest distribution. The high humidity and canopy water content make the northwest
343 Amazonian rainforest extremely resistant to fire spread (Cochrane & Barber, 2009).
344 However, savannas in the southern and eastern Amazonia, which experience seasonal
345 rainfall, are not effectively buffered from fire (Uhl, 1998). Savannas are naturally fire-prone
346 and adapted to frequent fire. Therefore, we found that as the forest loss rate increases, the fire
347 burn area stays relatively stable. Fire risk in seasonal forests is generally much lower than
348 surrounding savannas because of less-open canopy, lower mass of fuel, and higher litter
349 moisture (Bowman & Wilson, 1988).

350 Our results indicated that seasonal forests and the forests across the seasonal forest-
351 savanna boundary experienced much higher losses than northern rainforests and southern
352 savannas and are more susceptible to fire. Fires increased in more than half of the regions
353 which experienced forest cover losses larger than 10%. More than 80% of the regions where
354 forest cover losses greater than 40% experienced increases in fire. Forest canopy loss reduces
355 forest fuel moisture in the subcanopy and allows solar radiation to heat understory vegetation
356 and dry litter fuel (Messina & Cochrane, 2007). Forest loss due to either natural or
357 anthropogenic activities causes fragmentation, leading to ignition increases and fuel moisture
358 decreases (Alencar et al., 2015). Forest fragments are particularly vulnerable and fire-prone
359 because they are often adjacent to cattle pastures which are often logged and burned
360 (Laurance & Williamson, 2001).

361 We showed that forest loss modifies regional climate, and when superimposed on
362 climate change, can increase fire susceptibility and exacerbate regional drought. Intensive
363 drought interactions with fire causes large scale changes to canopy structure and composition,
364 and shifts forest to savanna-like or scrub vegetation (Balch et al., 2008; Hutyra et al.,
365 2005). The savanna-like vegetation is more flammable yet better fire adapted. Repeated
366 droughts that persist for years can cause vegetation mortality and amplify forest losses (Brando
367 et al., 2014; Saatchi et al., 2013; Zemp et al., 2017). The rising deforestation rate in recent years
368 (Qin et al., 2019) potentially increases droughts, forest fragments, and fire loads, and therefore
369 expands fire risk northward to the tropical seasonal forest. Efforts to promote forest
370 conservation and fire protection is a critical priority to prevent Amazonia from further climate
371 and fire regime shift that compromises regional sustainability.

372 **Data availability**

373 All reanalyses and satellite data used in this study are publicly available under the following URLs.

- 374 • Global Fire Emissions Database, Version 4.1 (GFEDv4):
375 https://daac.ornl.gov/VEGETATION/guides/fire_emissions_v4_R1.html
376 • ESA Fire Climate Change Initiative (Fire CCI) Dataset Collection:
377 <https://catalogue.ceda.ac.uk/uuid/4f377defc2454db9b2a6d032abfd0cbd>
378 • Global forest change (GFC v1.5):
379 https://earthenginepartners.appspot.com/science-2013-global-forest/download_v1.5.html
380 • MODIS Aqua 8-day Land Surface Temperature and Emissivity (LST&E) L3 Global products:
381 <https://ladsweb.modaps.eosdis.nasa.gov/missions-and-measurements/products/MYD11C2/>
382 • MODIS Bidirectional Reflectance Distribution Function and Albedo (BRDF/Albedo) dataset (MCD43C3
383 Version 6):
384 <https://lpdaac.usgs.gov/products/mcd43c3v006/>
385 • MODIS evapotranspiration and latent heat flux product (MOD16A2 Version 6):
386 <https://lpdaac.usgs.gov/products/mod16a2v006/>
387 • Clouds and the Earth's Radiant Energy System (CERES) Energy Balanced And Filled (EBAF)-Surface
388 Product:
389 <https://ceres.larc.nasa.gov/products-info.php?product=EBAF>
390 • MODIS Aqua 8-day Land Surface Temperature and Emissivity (LST&E) L3 Global products (MYD11C2
391 Version 6):
392 <https://lpdaac.usgs.gov/products/myd11c2v006/>
393 • Köppen-geiger climate classification at half-degree:
394 <http://koeppen-geiger.vu-wien.ac.at/present.htm>
395 • 0.5-degree Global Precipitation Climatology Centre (GPCC) monthly precipitation dataset:
396 <https://psl.noaa.gov/data/gridded/data.gpcc.html>
397 • 0.5-degree GHCN_CAMS Gridded 2m temperature:
398 <https://www.esrl.noaa.gov/psd/data/gridded/data.ghcncams.html>
399 • ECMWF ERA5 monthly reanalysis at 0.25-degree:
400 <https://www.ecmwf.int/en/forecasts/datasets/reanalysis-datasets/era5>
401 • half-degree Self-calibrating Palmer Drought Severity Index:
402 <https://crudata.uea.ac.uk/cru/data/drought/>
403

404 **Acknowledgements**

405 X. X., X.Z. and Y.X. were supported by the Natural Science Foundation of China
406 (#41875107) and National Key R&D Program of China (2018YFA0606002). G.J. was
407 supported by Strategic Priority Research Program of the Chinese Academy of Sciences,
408 CASEarth (XDA19030401). W.J.R. was supported by U.S. Department of Energy, Office of
409 Science, Biological and Environmental Research, Regional and Global Climate Modeling
410 Program through the RUBISCO Scientific Focus Area under contract DE-AC02-05CH11231
411 to Lawrence Berkeley National Laboratory.

412

413 **Competing interests**

414 The authors declare no conflicts of interest.

415 **Reference**

- 416 Agudelo, J., Arias, P. A., Vieira, S. C., & Martínez, J. A. (2019). Influence of longer dry
417 seasons in the Southern Amazon on patterns of water vapor transport over northern
418 South America and the Caribbean. *Climate Dynamics*, 52(5), 2647–2665.
419 <https://doi.org/10.1007/s00382-018-4285-1>
- 420 Alencar, A. A., Brando, P. M., Asner, G. P., & Putz, F. E. (2015). Landscape fragmentation,
421 severe drought, and the new Amazon forest fire regime. *Ecological Applications*, 25(6),
422 1493–1505. <https://doi.org/10.1890/14-1528.1>
- 423 Bagley, J. E., Desai, A. R., Harding, K. J., Snyder, P. K., & Foley, J. A. (2013). Drought and
424 Deforestation: Has Land Cover Change Influenced Recent Precipitation Extremes in the
425 Amazon? *Journal of Climate*, 27(1), 345–361. <https://doi.org/10.1175/JCLI-D-12-00369.1>
- 427 Bala, G., Caldeira, K., Wickett, M., Phillips, T. J., Lobell, D. B., Delire, C., & Mirin, A.
428 (2007). Combined climate and carbon-cycle effects of large-scale deforestation.
429 *Proceedings of the National Academy of Sciences of the United States of America*,
430 104(16), 6550–6555. <https://doi.org/10.1073/pnas.0608998104>
- 431 Balch, J. R. K., Nepstad, D. C., Brando, P. M., Curran, L. M., Portela, O., de Carvalho, O., &
432 Lefebvre, P. (2008). Negative fire feedback in a transitional forest of southeastern
433 Amazonia. *Global Change Biology*, 14(10), 2276–2287. <https://doi.org/10.1111/j.1365-2486.2008.01655.x>
- 435 Barichivich, J., Gloor, E., Peylin, P., Brienen, R. J. W., Schöngart, J., Espinoza, J. C., &
436 Pattanayak, K. C. (2018). Recent intensification of Amazon flooding extremes driven by
437 strengthened Walker circulation. *Science Advances*, 4(9), eaat8785.
438 <https://doi.org/10.1126/sciadv.aat8785>
- 439 Barichivich, J., Osborn, T. J., Harris, I., van der Schrier, G., & Jones, P. D. (2019). Drought
440 [in “State of the Climate in 2018”]. *Bulletin of the American Meteorological Society*,
441 100, S39–S40. <https://doi.org/10.1175/2019BAMSSStateoftheClimate.1>
- 442 Beck, H. E., Zimmermann, N. E., McVicar, T. R., Vergopolan, N., Berg, A., & Wood, E. F.
443 (2018). Present and future Köppen-Geiger climate classification maps at 1-km
444 resolution. *Scientific Data*, 5, 180214. Retrieved from
445 <https://doi.org/10.1038/sdata.2018.214>
- 446 Bowman, D. M. J. S., & Wilson, B. A. (1988). Fuel Characteristics of Coastal Monsoon
447 Forests, Northern Territory, Australia. *Journal of Biogeography*, 15(5/6), 807–817.
448 <https://doi.org/10.2307/2845341>
- 449 Bradshaw, C. J. A., Sodhi, N. S., Peh, K. S. H., & Brook, B. W. (2007). Global evidence that
450 deforestation amplifies flood risk and severity in the developing world. *Global Change*
451 *Biology*, 13(11), 2379–2395. <https://doi.org/10.1111/j.1365-2486.2007.01446.x>
- 452 Brando, P. M., Balch, J. K., Nepstad, D. C., Morton, D. C., Putz, F. E., Coe, M. T., ...
453 Soares-Filho, B. S. (2014). Abrupt increases in Amazonian tree mortality due to
454 drought-fire interactions. *Proceedings of the National Academy of Sciences*, 111(17),
455 6347–6352. <https://doi.org/10.1073/pnas.1305499111>
- 456 Cavalcante, R. B. L., Pontes, P. R. M., Souza-Filho, P. W. M., & de Souza, E. B. (2019).
457 Opposite Effects of Climate and Land Use Changes on the Annual Water Balance in the
458 Amazon Arc of Deforestation. *Water Resources Research*, 55(4), 3092–3106.
459 <https://doi.org/10.1029/2019WR025083>
- 460 Chambers, J. Q., & Artaxo, P. (2017). Deforestation size influences rainfall. *Nature Climate*
461 *Change*, 7(3), 175–176. <https://doi.org/10.1038/nclimate3238>
- 462 Christensen, J. H., Kumar, K. K., Aldrian, E., An, S.-I., Cavalcanti, I. F. A., Castro, M. de, ...
463 Zhou, T. (2013). Climate Phenomena and their Relevance for Future Regional Climate
464 Change. In T. F. Stocker, D. Qin, G.-K. Plattner, M. Tignor, S. K. Allen, J.

465 Boschung, ... P. M. Midgley (Eds.), *Climate Change 2013: The Physical Science Basis.*
466 *Contribution of Working Group I to the Fifth Assessment Report of the*
467 *Intergovernmental Panel on Climate Change.* Cambridge, United Kingdom and New
468 York, NY, USA.: Cambridge University Press.

469 Clark, C. (1987). Deforestation and Floods. *Environmental Conservation*, 14(1), 67–69.
470 <https://doi.org/DOI: 10.1017/S0376892900011127>

471 Cochrane, M. A., & Barber, C. P. (2009). Climate change, human land use and future fires in
472 the Amazon. *Global Change Biology*, 15(3), 601–612. [https://doi.org/10.1111/j.1365-](https://doi.org/10.1111/j.1365-2486.2008.01786.x)
473 [2486.2008.01786.x](https://doi.org/10.1111/j.1365-2486.2008.01786.x)

474 Coe, M. T., Costa, M. H., & Soares-Filho, B. S. (2009). The influence of historical and
475 potential future deforestation on the stream flow of the Amazon River – Land surface
476 processes and atmospheric feedbacks. *Journal of Hydrology*, 369(1), 165–174.
477 <https://doi.org/https://doi.org/10.1016/j.jhydrol.2009.02.043>

478 D’Almeida, C., Vörösmarty, C. J., Hurtt, G. C., Marengo, J. A., Dingman, S. L., & Keim, B.
479 D. (2007). The effects of deforestation on the hydrological cycle in Amazonia: a review
480 on scale and resolution. *International Journal of Climatology*, 27(5), 633–647.
481 <https://doi.org/10.1002/joc.1475>

482 Davidson, E. A., De Araújo, A. C., Artaxo, P., Balch, J. K., Brown, I. F., Mercedes, M.
483 M., ... Wofsy, S. C. (2012). The Amazon basin in transition. *Nature*, 481(7381), 321–
484 328. <https://doi.org/10.1038/nature10717>

485 Ellison, D., Morris, C. E., Locatelli, B., Sheil, D., Cohen, J., Murdiyarso, D., ... Sullivan, C.
486 A. (2017). Trees, forests and water: Cool insights for a hot world. *Global Environmental*
487 *Change*, 43, 51–61. <https://doi.org/10.1016/j.gloenvcha.2017.01.002>

488 ERA5. (2019). *ERA5 Reanalysis (0.25 Degree Latitude-Longitude Grid)*.
489 <https://doi.org/10.5065/BH6N-5N20>

490 Erfanian, A., Wang, G., & Fomenko, L. (2017). Unprecedented drought over tropical South
491 America in 2016: Significantly under-predicted by tropical SST. *Scientific Reports*, 7(1),
492 5811. <https://doi.org/10.1038/s41598-017-05373-2>

493 Espinoza, J. C., Ronchail, J., Marengo, J. A., & Segura, H. (2019). Contrasting North–South
494 changes in Amazon wet-day and dry-day frequency and related atmospheric features
495 (1981–2017). *Climate Dynamics*, 52(9), 5413–5430. [https://doi.org/10.1007/s00382-](https://doi.org/10.1007/s00382-018-4462-2)
496 [018-4462-2](https://doi.org/10.1007/s00382-018-4462-2)

497 Fan, Y., & van den Dool, H. (2008). A global monthly land surface air temperature analysis
498 for 1948–present. *Journal of Geophysical Research: Atmospheres*, 113(D1).
499 <https://doi.org/10.1029/2007JD008470>

500 Fu, R., Yin, L., Li, W., Arias, P. A., Dickinson, R. E., Huang, L., ... Myneni, R. B. (2013).
501 Increased dry-season length over southern Amazonia in recent decades and its
502 implication for future climate projection. *Proceedings of the National Academy of*
503 *Sciences*, 110(45), 18110 LP – 18115. <https://doi.org/10.1073/pnas.1302584110>

504 Gentry, A. H., & Lopez-Parodi, J. (1980). Deforestation and increased flooding of the upper
505 amazon. *Science*, 210(4476), 1354–1356. <https://doi.org/10.1126/science.210.4476.1354>

506 Gimeno, L., Dominguez, F., Nieto, R., Trigo, R., Drumond, A., Reason, C. J. C., ...
507 Marengo, J. (2016). Major Mechanisms of Atmospheric Moisture Transport and Their
508 Role in Extreme Precipitation Events. *Annual Review of Environment and Resources*,
509 41(1), 117–141. <https://doi.org/10.1146/annurev-environ-110615-085558>

510 Gloor, M., Brienen, R. J. W., Galbraith, D., Feldpausch, T. R., Schöngart, J., Guyot, J.-L., ...
511 Phillips, O. L. (2013). Intensification of the Amazon hydrological cycle over the last two
512 decades. *Geophysical Research Letters*, 40(9), 1729–1733.
513 <https://doi.org/10.1002/grl.50377>

514 Hansen, M. C., Potapov, P. V., Moore, R., Hancher, M., Turubanova, S. A., Tyukavina,

515 A., ... Townshend, J. R. G. (2013). High-resolution global maps of 21st-century forest
516 cover change. *Science*, 342(6160), 850–853. <https://doi.org/10.1126/science.1244693>

517 Hirota, M., Holmgren, M., Van Nes, E. H., & Scheffer, M. (2011). Global Resilience of
518 Tropical Forest and Savanna to Critical Transitions. *Science*, 334(6053), 232 LP – 235.
519 <https://doi.org/10.1126/science.1210657>

520 Hutyra, L. R., Munger, J. W., Nobre, C. A., Saleska, S. R., Vieira, S. A., & Wofsy, S. C.
521 (2005). Climatic variability and vegetation vulnerability in Amazônia. *Geophysical*
522 *Research Letters*, 32(24). <https://doi.org/10.1029/2005GL024981>

523 Jiménez-Muñoz, J. C., Mattar, C., Barichivich, J., Santamaría-Artigas, A., Takahashi, K.,
524 Malhi, Y., ... Schrier, G. van der. (2016, December 8). Record-breaking warming and
525 extreme drought in the Amazon rainforest during the course of El Niño 2015-2016.
526 *Scientific Reports*, Vol. 6, p. 33130. <https://doi.org/10.1038/srep33130>

527 Laurance, W. F., Camargo, J. L. C., Fearnside, P. M., Lovejoy, T. E., Williamson, G. B.,
528 Mesquita, R. C. G., ... Laurance, S. G. W. (2018). An Amazonian rainforest and its
529 fragments as a laboratory of global change. *Biological Reviews*, 93(1), 223–247.
530 <https://doi.org/10.1111/brv.12343>

531 Laurance, W. F., & Williamson, G. B. (2001). Positive Feedbacks among Forest
532 Fragmentation, Drought, and Climate Change in the Amazon. *Conservation Biology*,
533 15(6), 1529–1535. <https://doi.org/10.1046/j.1523-1739.2001.01093.x>

534 Lawrence, D., & Vandecar, K. (2015). Effects of tropical deforestation on climate and
535 agriculture. *Nature Climate Change*, 5(1), 27–36. <https://doi.org/10.1038/nclimate2430>

536 Li, Y., Zhao, M., Motesharrei, S., Mu, Q., Kalnay, E., & Li, S. (2015). Local cooling and
537 warming effects of forests based on Satellite Observations. *Nature Communications*, 6,
538 1–8. <https://doi.org/10.1038/ncomms7603>

539 Lloyd, J., Goulden, M. L., Ometto, J. P., Patiño, S., Fyllas, N. M., & Quesada, C. A. (2009,
540 January 1). Ecophysiology of Forest and Savanna Vegetation. *Amazonia and Global*
541 *Change*, pp. 463–484. <https://doi.org/doi:10.1029/2008GM000741>

542 Malhi, Y., Aragao, L. E. O. C., Galbraith, D., Huntingford, C., Fisher, R., Zelazowski, P., ...
543 Meir, P. (2009). Exploring the likelihood and mechanism of a climate-change-induced
544 dieback of the Amazon rainforest. *Proceedings of the National Academy of Sciences*,
545 106(49), 20610–20615. <https://doi.org/10.1073/pnas.0804619106>

546 Malhi, Yadvinder, Roberts, J. T., Betts, R. A., Killeen, T. J., Li, W., & Nobre, C. A. (2008).
547 Climate Change, Deforestation, and the Fate of the Amazon. *Science*, 319(5860), 169
548 LP – 172. <https://doi.org/10.1126/science.1146961>

549 Messina, J. P., & Cochrane, M. A. (2007). The Forests are Bleeding: How land use change is
550 creating a new fire regime in the Ecuadorian Amazon. *Journal of Latin American*
551 *Geography*, 6(1), 85–100. Retrieved from <http://www.jstor.org/stable/25765159>

552 Negrón-Juárez, R. I., Holm, J. A., Marra, D. M., Rifai, S. W., Riley, W. J., Chambers, J.
553 Q., ... Higuchi, N. (2018). Vulnerability of Amazon forests to storm-driven tree
554 mortality. *Environmental Research Letters*, 13(5), 54021. <https://doi.org/10.1088/1748-9326/aabe9f>

555

556 Nepstad, D. C., Tohver, I. M., David, R., Moutinho, P., & Cardinot, G. (2007). Mortality of
557 large trees and lianas following experimental drought in an amazon forest. *Ecology*,
558 88(9), 2259–2269. <https://doi.org/10.1890/06-1046.1>

559 Nepstad, D., Lefebvre, P., Lopes da Silva, U., Tomasella, J., Schlesinger, P., Solórzano,
560 L., ... Guerreira Benito, J. (2004). Amazon drought and its implications for forest
561 flammability and tree growth: a basin-wide analysis. *Global Change Biology*, 10(5),
562 704–717. <https://doi.org/10.1111/j.1529-8817.2003.00772.x>

563 Nobre, C. A., Sampaio, G., Borma, L. S., Castilla-Rubio, J. C., Silva, J. S., & Cardoso, M.
564 (2016). Land-use and climate change risks in the amazon and the need of a novel

565 sustainable development paradigm. *Proceedings of the National Academy of Sciences of*
566 *the United States of America*, 113(39), 10759–10768.
567 <https://doi.org/10.1073/pnas.1605516113>

568 Otón, G., Ramo, R., Lizundia-Loiola, J., & Chuvieco, E. (2019). Global Detection of Long-
569 Term (1982–2017) Burned Area with AVHRR-LTDR Data. *Remote Sensing*, Vol. 11.
570 <https://doi.org/10.3390/rs11182079>

571 Palmer, W. C. (1965). *Meteorological drought*. [https://doi.org/Technique Report Weather](https://doi.org/Technique%20Report%20Weather%20Bureau%20Research%20Paper%20No.%2045)
572 Bureau Research Paper No. 45

573 Phillips, O. L., van der Heijden, G., Lewis, S. L., López-González, G., Aragão, L. E. O. C.,
574 Lloyd, J., ... Vilanova, E. (2010). Drought–mortality relationships for tropical forests.
575 *New Phytologist*, 187(3), 631–646. <https://doi.org/10.1111/j.1469-8137.2010.03359.x>

576 Qin, Y., Xiao, X., Dong, J., Zhang, Y., Wu, X., Shimabukuro, Y., ... Moore, B. (2019).
577 Improved estimates of forest cover and loss in the Brazilian Amazon in 2000–2017.
578 *Nature Sustainability*, 2(8), 764–772. <https://doi.org/10.1038/s41893-019-0336-9>

579 Randerson, J. T., Werf, G. R. van der, Giglio, L., Collatz, G. J., & Kasibhatla., P. S. (2018).
580 *Global Fire Emissions Database, Version 4.1 (GFEDv4)*. Oak Ridge, Tennessee, USA.

581 Running, S., Mu, Q., & Zhao, M. (2017). *MOD16A2 MODIS/Terra Net Evapotranspiration*
582 *8-Day L4 Global 500m SIN Grid V006*. <https://doi.org/10.5067/MODIS/MOD16A2.006>

583 Saatchi, S., Asefi-Najafabady, S., Malhi, Y., Aragão, L. E. O. C., Anderson, L. O., Myneni,
584 R. B., & Nemani, R. (2013). Persistent effects of a severe drought on Amazonian forest
585 canopy. *Proceedings of the National Academy of Sciences*, 110(2), 565 LP – 570.
586 <https://doi.org/10.1073/pnas.1204651110>

587 Schaaf, C., & Wang, Z. (2015). *MCD43C3 MODIS/Terra+Aqua BRDF/Albedo Albedo Daily*
588 *L3 Global 0.05Deg CMG V006*. <https://doi.org/10.5067/MODIS/MCD43C3.006>

589 Schneider, U., Becker, A., Finger, P., Meyer-Christoffer, A., Rudolf, B., & Ziese, M. (2011).
590 *GPCC Full Data Reanalysis Version 6.0 at 0.5°: Monthly Land-Surface Precipitation*
591 *from Rain-Gauges built on GTS-based and Historic Data*.
592 https://doi.org/10.5676/DWD_GPCC/FD_M_V7_050

593 Skansi, M. de los M., Brunet, M., Sigró, J., Aguilar, E., Arevalo Groening, J. A., Bentancur,
594 O. J., ... Jones, P. D. (2013). Warming and wetting signals emerging from analysis of
595 changes in climate extreme indices over South America. *Global and Planetary Change*,
596 100, 295–307. <https://doi.org/https://doi.org/10.1016/j.gloplacha.2012.11.004>

597 Staal, A., Flores, B. M., Aguiar, A. P. D., Bosmans, J. H. C., Fetzer, I., & Tuinenburg, O. A.
598 (2020). Feedback between drought and deforestation in the Amazon. *Environmental*
599 *Research Letters*, 15(4), 44024. <https://doi.org/10.1088/1748-9326/ab738e>

600 Staal, A., Tuinenburg, O. A., Bosmans, J. H. C., Holmgren, M., Van Nes, E. H., Scheffer,
601 M., ... Dekker, S. C. (2018). Forest-rainfall cascades buffer against drought across the
602 Amazon. *Nature Climate Change*, 8(6), 539–543. [https://doi.org/10.1038/s41558-018-](https://doi.org/10.1038/s41558-018-0177-y)
603 0177-y

604 Stephens, S. L., Collins, B. M., Fettig, C. J., Finney, M. A., Hoffman, C. M., Knapp, E. E., ...
605 Wayman, R. B. (2018). Drought, Tree Mortality, and Wildfire in Forests Adapted to
606 Frequent Fire. *BioScience*, 68(2), 77–88. <https://doi.org/10.1093/biosci/bix146>

607 Taufik, M., Torfs, P. J. J. F., Uijlenhoet, R., Jones, P. D., Murdiyarso, D., & Van Lanen, H.
608 A. J. (2017). Amplification of wildfire area burnt by hydrological drought in the humid
609 tropics. *Nature Climate Change*, 7, 428. Retrieved from
610 <http://dx.doi.org/10.1038/nclimate3280>

611 Trenberth, K. E., Dai, A., Van Der Schrier, G., Jones, P. D., Barichivich, J., Briffa, K. R., &
612 Sheffield, J. (2014). Global warming and changes in drought. *Nature Climate Change*,
613 4(1), 17–22. <https://doi.org/10.1038/nclimate2067>

614 Uhl, C. (1998). Perspectives on Wildfire in the Humid Tropics. *Conservation Biology*, 12(5),

615 942–943. <https://doi.org/10.1046/j.1523-1739.1998.012005942.x>

616 Uhl, C., & Kauffman, J. B. (1990). Deforestation, Fire Susceptibility, and Potential Tree
617 Responses to Fire in the Eastern Amazon. *Ecology*, *71*(2), 437–449.
618 <https://doi.org/10.2307/1940299>

619 van der Schrier, G., Barichivich, J., Briffa, K. R., & Jones, P. D. (2013). A scPDSI-based
620 global data set of dry and wet spells for 1901–2009. *Journal of Geophysical Research:*
621 *Atmospheres*, *118*(10), 4025–4048. <https://doi.org/10.1002/jgrd.50355>

622 Wan, Z., Hook, S., & Hulley, G. (2015). *MYD11C2 MODIS/Aqua Land Surface*
623 *Temperature/Emissivity 8-Day L3 Global 0.05Deg CMG V006. 2015.*
624 <https://doi.org/10.5067/MODIS/MYD11C2.006>

625 Wright, J. S., Fu, R., Worden, J. R., Chakraborty, S., Clinton, N. E., Risi, C., ... Yin, L.
626 (2017). Rainforest-initiated wet season onset over the southern Amazon. *Proceedings of*
627 *the National Academy of Sciences*, *114*(32), 8481 LP – 8486.
628 <https://doi.org/10.1073/pnas.1621516114>

629 Yoon, J.-H., & Zeng, N. (2010). An Atlantic influence on Amazon rainfall. *Climate*
630 *Dynamics*, *34*(2), 249–264. <https://doi.org/10.1007/s00382-009-0551-6>

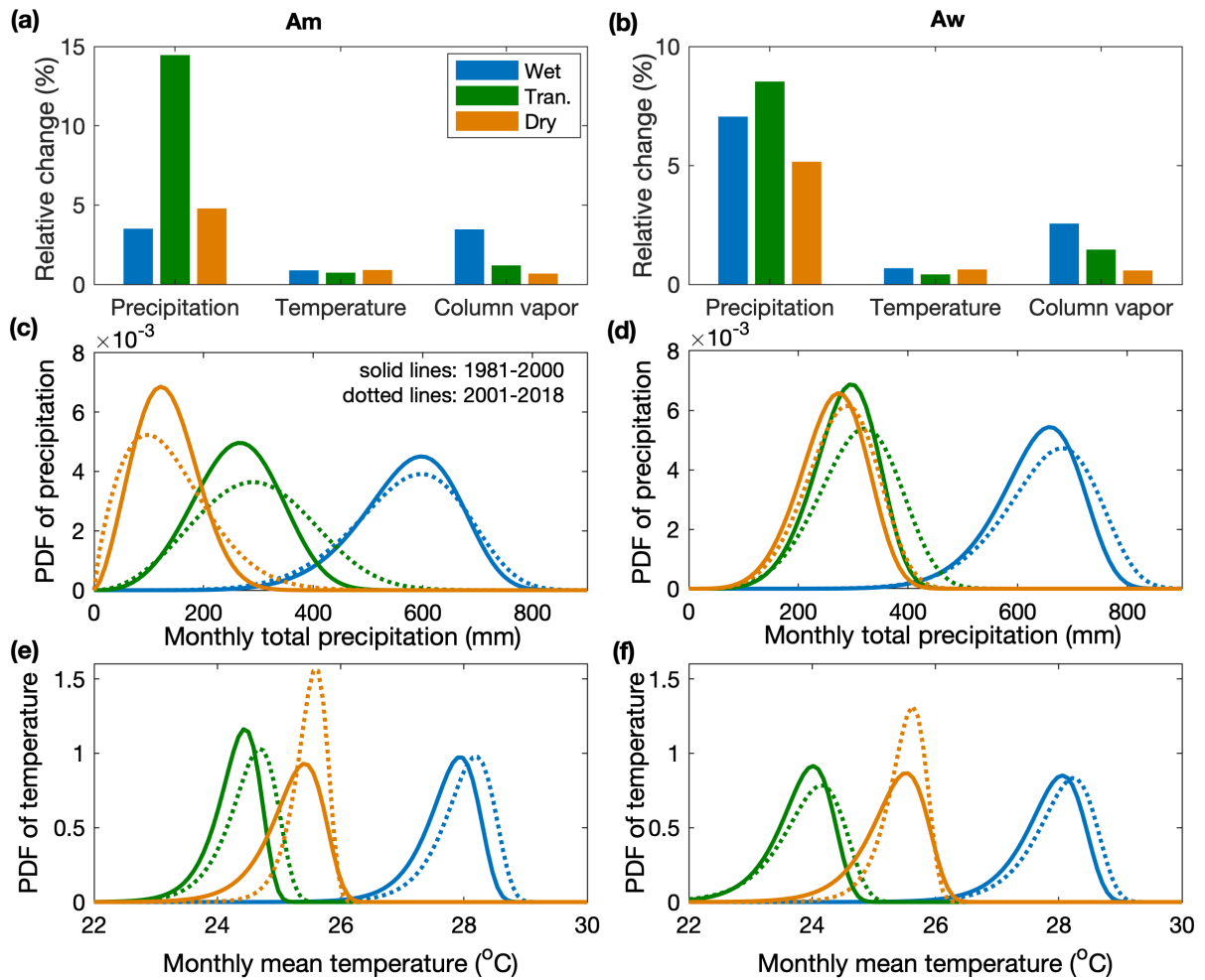
631 Zemp, D. C., Schleussner, C. F., Barbosa, H. M. J., Hirota, M., Montade, V., Sampaio, G., ...
632 Rammig, A. (2017). Self-amplified Amazon forest loss due to vegetation-atmosphere
633 feedbacks. *Nature Communications*, *8*, 1–10. <https://doi.org/10.1038/ncomms14681>

634 Zeng, N., Yoon, J.-H., Marengo, J. A., Subramaniam, A., Nobre, C. A., Mariotti, A., &
635 Neelin, J. D. (2008). Causes and impacts of the 2005 Amazon drought. *Environmental*
636 *Research Letters*, *3*(1), 14002. <https://doi.org/10.1088/1748-9326/3/1/014002>

637 Zhang, M., Liu, N., Harper, R., Li, Q., Liu, K., Wei, X., ... Liu, S. (2017). A global review
638 on hydrological responses to forest change across multiple spatial scales: Importance of
639 scale, climate, forest type and hydrological regime. *Journal of Hydrology*, *546*, 44–59.
640 <https://doi.org/https://doi.org/10.1016/j.jhydrol.2016.12.040>

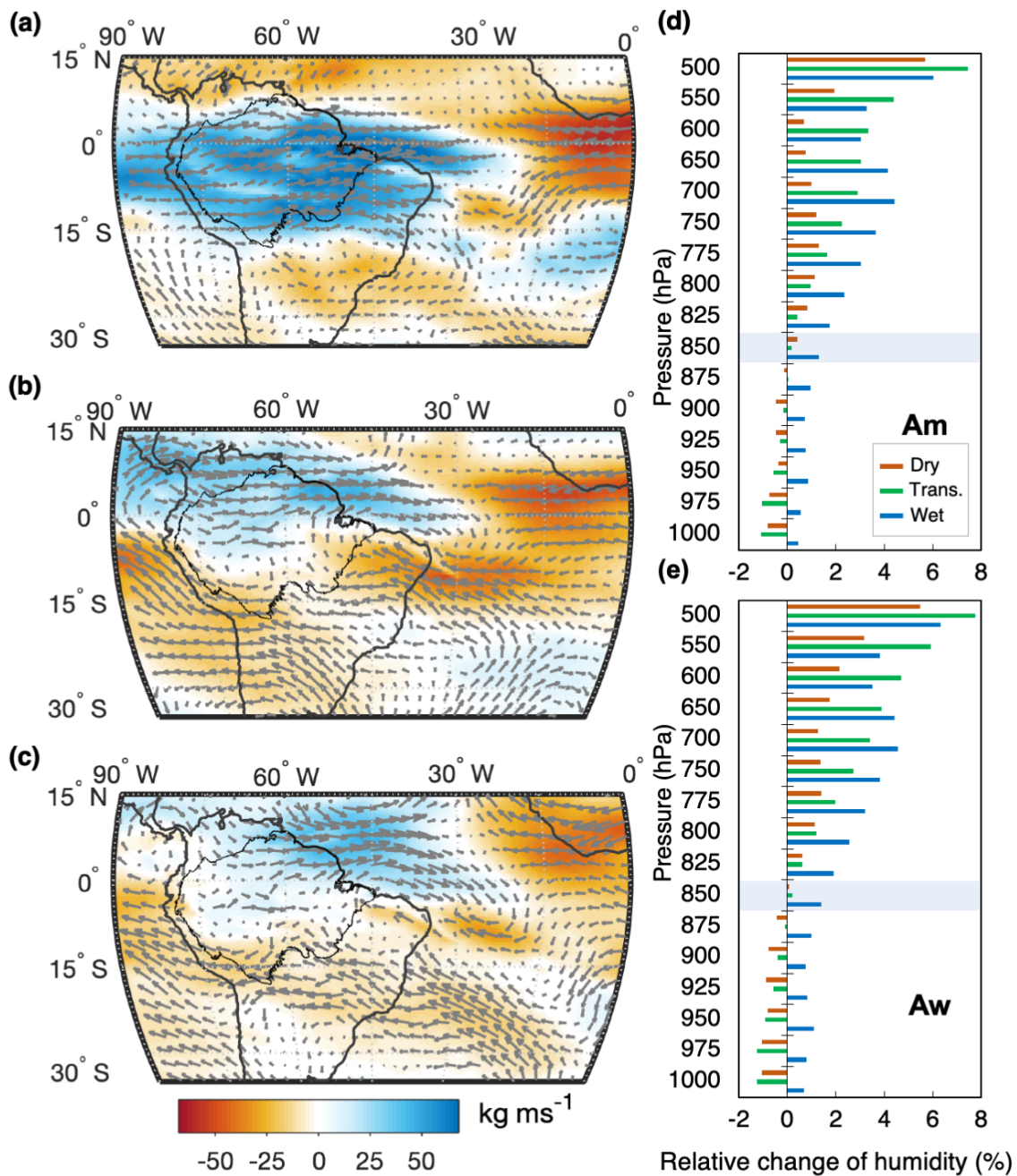
641

642

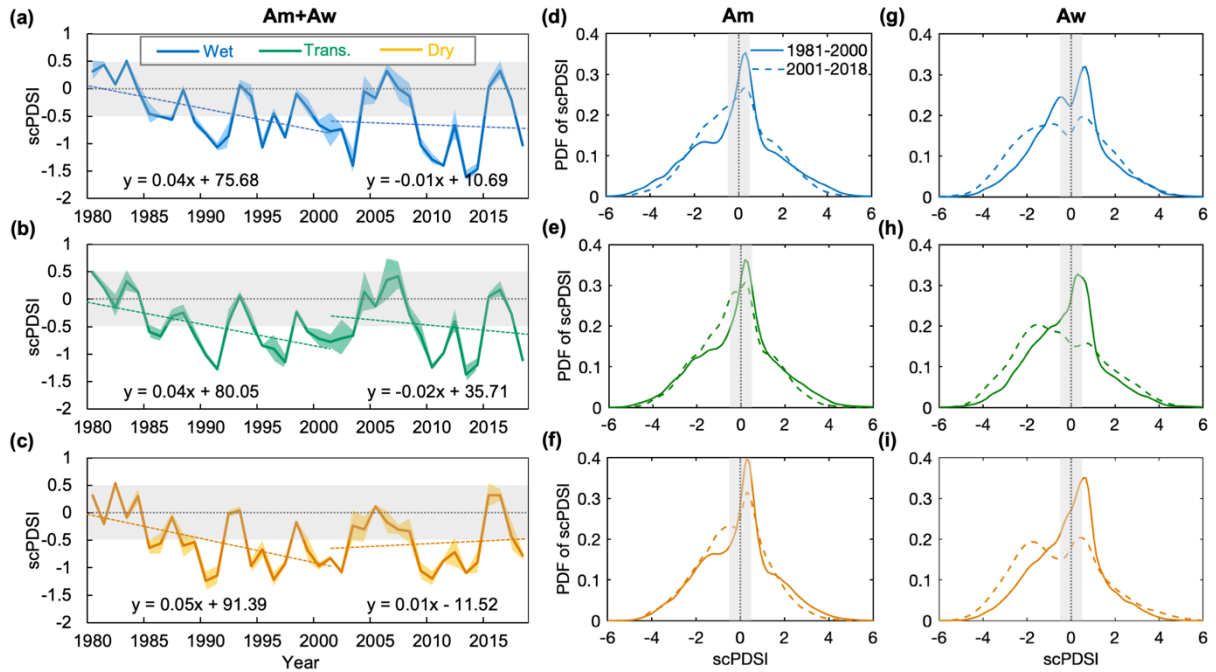


643
 644
 645
 646
 647
 648
 649
 650

Figure 1: Climate regime shift of in Amazon monsoon (Am) and winter dry (Aw) climates. The relative change (%) of precipitation, temperature, and total column water vapor during 2001-2018 relative to that in 1981-2000 for Am (a) and Aw (b), probability distribution functions of precipitation for Am (c) and Aw (d), and probability distribution functions of temperature for Am (e) and Aw (f) for wet season, transition season and dry season. The solid and dotted lines in (c-f) denote probability distribution functions for precipitation (c and d) and temperature (e and f) in 1981-2000 and 2001-2018, respectively.

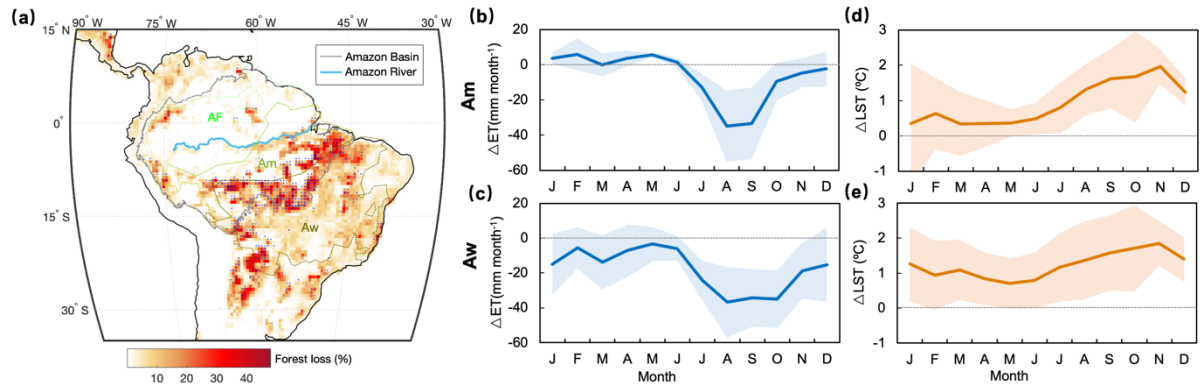


651
 652 **Figure 2: Changes in vertically integrated eastward water vapor fluxes and vertical**
 653 **profiles of water vapor change.** Vertically integrated eastward water vapor fluxes (kg ms^{-1})
 654 change in 2000-2018 in relative to 1981-2000 for (a) dry season, (b) transition season and (c)
 655 wet season. The vertical profiles of relative change (%) in specific humidity between 2001-
 656 2018 and 1981-2000 for wet, transition, and dry season in tropical monsoon climate region
 657 (d) and tropical winter dry climate region (e). The vectors in a-c denote the horizontal wind
 658 change between 1981-2000 and 2001-2018 at 850 hpa. The height of 850 hpa is shaded in d
 659 and e. The water vapor fluxes and vertical profiles were plotted with ERA5 monthly
 660 reanalysis.

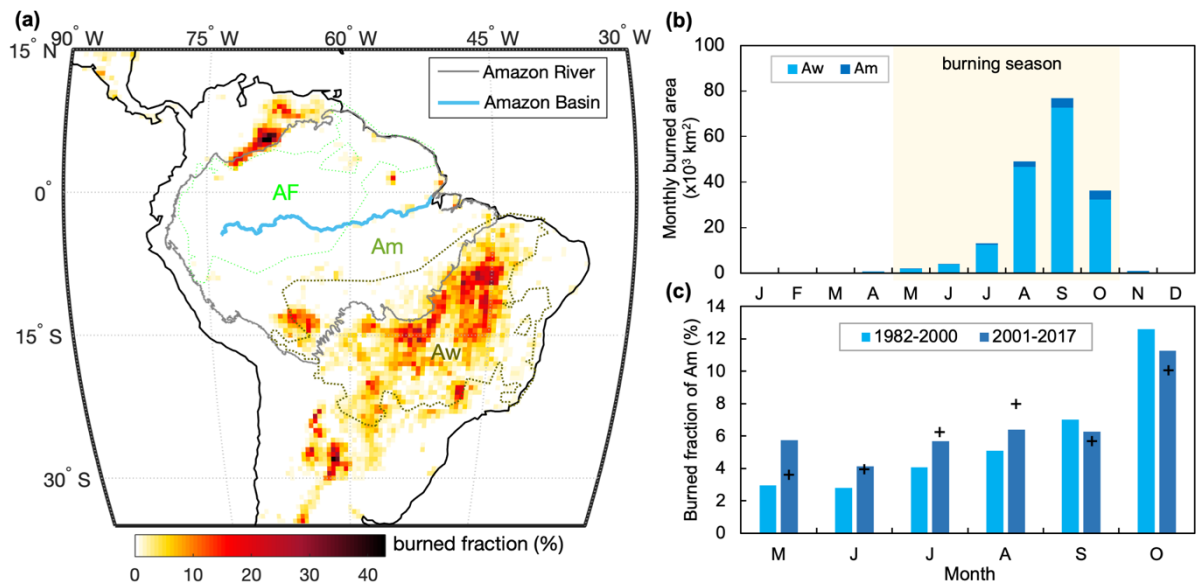


661
 662
 663
 664
 665
 666
 667
 668
 669
 670

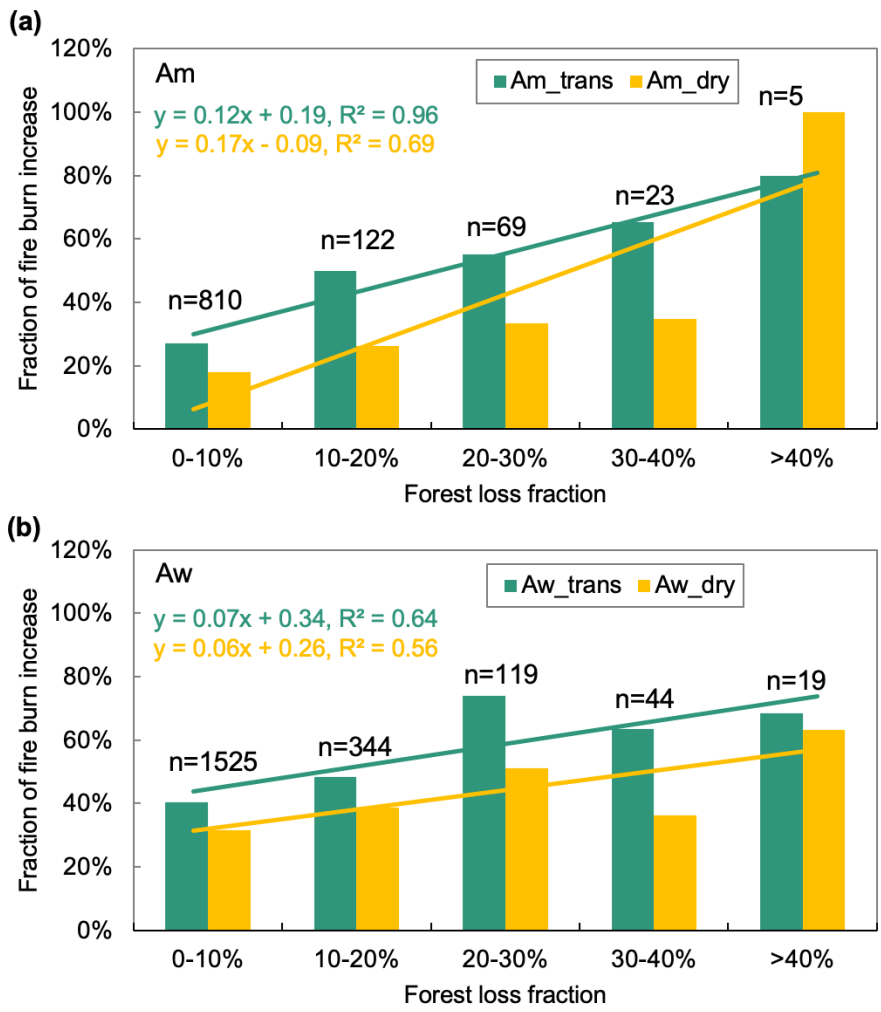
Figure 3: Drought conditions between 1980 and 2018 across the tropical monsoon climate and winter dry climate regions. Time series of *self-calibrating* Palmer Drought Severity Index (scPDSI) in wet (a), transition (b), and dry (c) seasons and the probability distribution functions of scPDSI in the wet, transition, and dry season for tropical monsoon climate region (d, e and f) and tropical winter dry climate region (g, h and i). The shaded pattern surrounding the time series (a-c) denote the standard deviation of scPDSI in each season. The solid and dashed lines in d-i denote the period 1981-2000 and 2001-2018, respectively. The grey shaded regions in a-i denote near-normal dryness condition ($-0.5 < \text{scPDSI} < 0.5$).



671
 672 **Figure 4: Forest loss and affected regional evapotranspiration and land surface**
 673 **temperature.** Accumulative forest loss (F_{loss} , %) during 2000-2017 in each $0.5 \times 0.5^\circ$ gridcell
 674 according to global forest change dataset (a), the blue dots denote the gridcells with both
 675 large forest loss ($F_{\text{loss}} > 65\%$) and pristine forest ($F_{\text{loss}} < 5\%$) between 2001 and 2017, monthly
 676 evapotranspiration change (ΔET , mm month^{-1}) due to accumulated forest loss in Am (b) and
 677 Aw (c), and monthly mean land surface temperature change (ΔLST , $^\circ\text{C}$) due to accumulated
 678 forest loss in Am (d) and Aw (e).. The shaded patterns in b-e are standard deviation of ΔET
 679 and ΔLST in gridcells with both large forest loss ($F_{\text{loss}} > 65\%$) and pristine forest ($F_{\text{loss}} < 5\%$)
 680 between 2000 and 2017.



681
 682 **Figure 5: The spatial and seasonal distribution of fire in Amazonia.** The annual mean
 683 fraction of fire burn in Amazon region between 1982 and 2017 based on ESA Fire Climate
 684 Change Initiative (Fire CCI) Dataset Collection (a). The dotted lines denote the major
 685 boundaries of Köppen-Geiger climate zones of tropical rainforest (Af), tropical monsoon
 686 climate (Am), and tropical winter dry climate (Aw). The mean seasonal distribution of
 687 burned area in tropical monsoon region (Am) and tropical winter dry region (Aw) during
 688 1982-2017 (b) and the fraction of burned area in Am and Aw that occurred in Am between
 689 May and October during 1982-2000 and 2001-2017 periods (c). The black + symbols in (c)
 690 denote the fraction of burned area in Am over the entire Am and Aw regions between May
 691 and October during 2001-2016 calculated from Global Fire Emissions Database, Version 4.1
 692 (GFEDv4).



693
694
695
696
697
698

Figure 6: Fraction of burned area increase is largely dependent on the fraction of forest loss. a. fraction of increased burned area against fraction of forest loss in tropical monsoon region (Am) for transitional and dry seasons and (b) fraction of burned area increase against fraction of forest loss in tropical winter dry region (Aw) for transitional and dry seasons. n is the total number of gridcells for each category of forest loss fraction.

699

Supplementary Information for
Climate regime shift and forest loss amplify fire in Amazonian forests

700

Table S1-S2

Figure S1-S4

701

Table S1: scPDSI defined dry and wet conditions

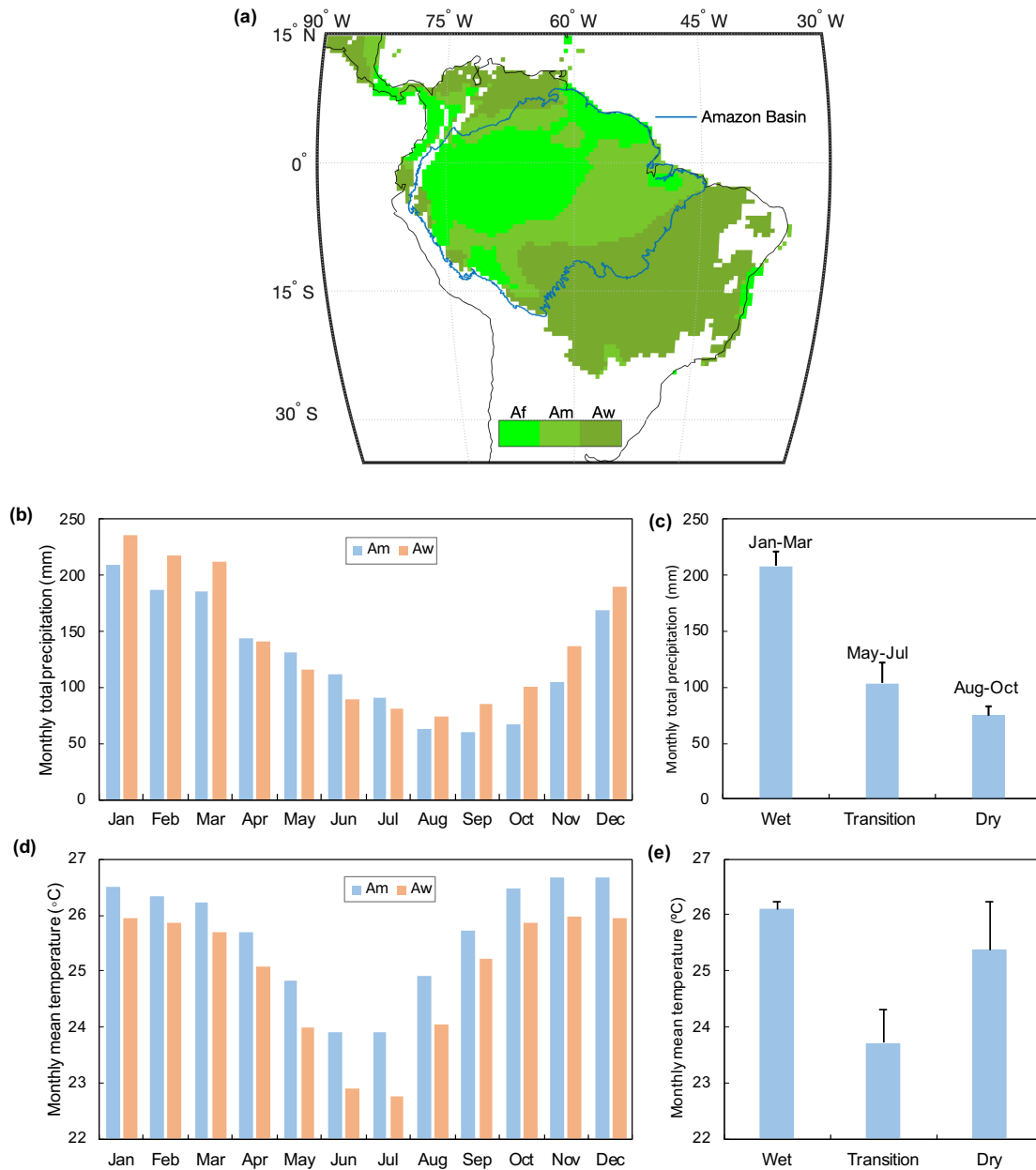
scPDSI range	Dry and wet condition
≥ 4.0	extremely wet
[3.0 4.0]	severely wet
[2.0 3.0]	moderately wet
[1.0 2.0]	slightly wet
[0.5 1.0]	incipient wet spell
[-0.5 0.5]	near normal
[-1.0 -0.5]	incipient dry spell
[-2.0 -1.0]	slightly dry
[-3.0 -2.0]	moderately dry
[-4.0 -3.0]	severely dry
≤ -4.0	extremely dry

702

703 **Table S2:** The total burned area in Am and Af and burned fraction of Am for
 704 two datasets: ESA_CCI and GFED.

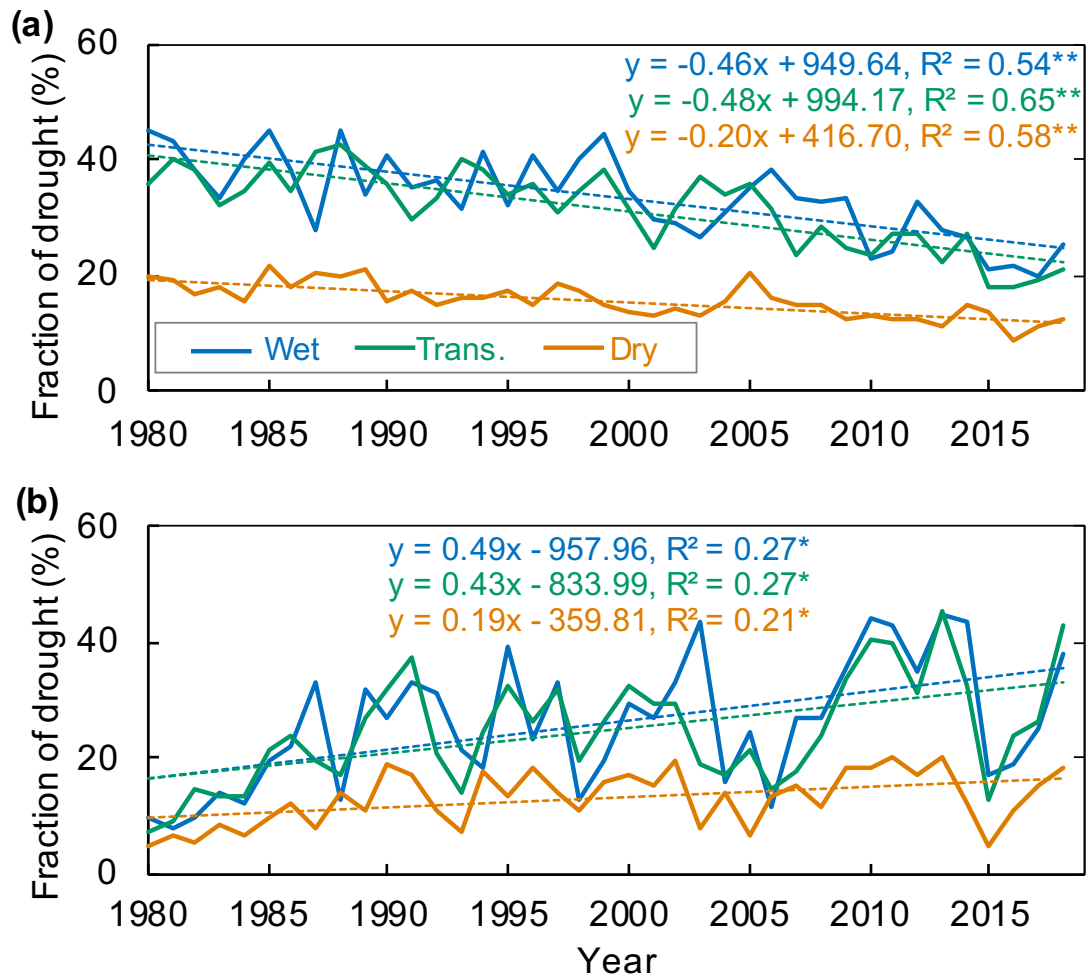
Data collection	ESA_cci		GFED
Period	1982-2017	1996-2016	1996-2016
Annual burned area in Am and Aw ($\times 10^3$ km ²)	178.5 \pm 65.4	182.4 \pm 66.0	148.5 \pm 72.0
Annual burned fraction in Am (%)	7.09 \pm 5.07	6.88 \pm 3.06	7.07 \pm 2.72

705



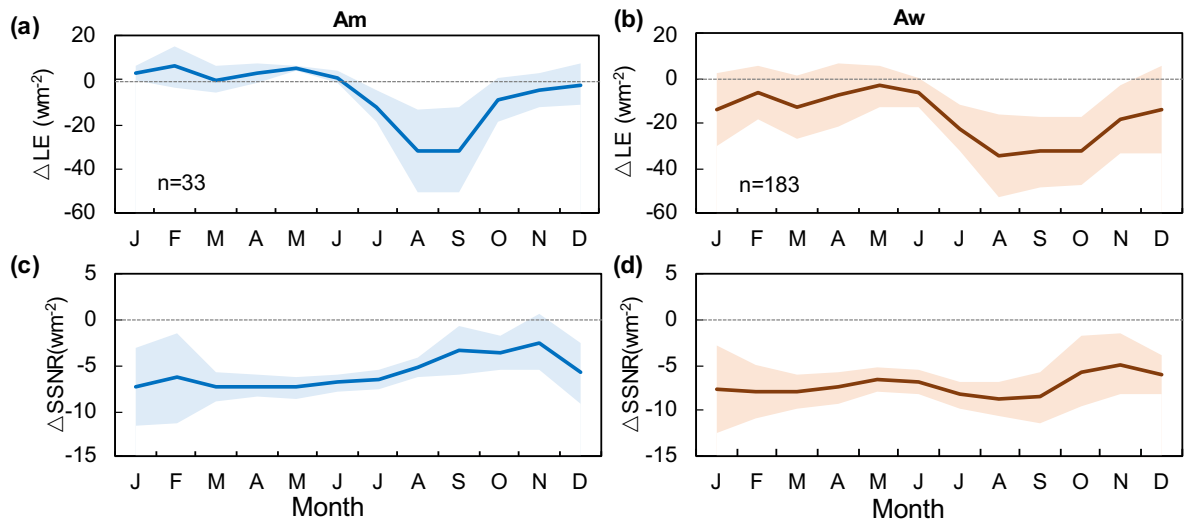
706
707
708
709
710
711
712
713
714

Figure S1: Amazonia climates and normal climate in tropical monsoon and tropical winter dry climate regions. The distribution of tropical rainforest (Af), tropical monsoon (Am) and tropical winter dry (Aw) climates (a), monthly total precipitation averaged over 1961-1990 in Am and Aw (b), monthly mean temperature averaged over 1961-1990 in Am and Aw (c), the monthly total precipitation in wet season (January-March), transition season (May-July) and dry season (August-October) for both Am and Aw (d), and monthly mean temperature in wet, transition and dry season for both Am and Aw (e). The normal climate of precipitation and temperature is only calculated for Am and Aw in the south of Af.



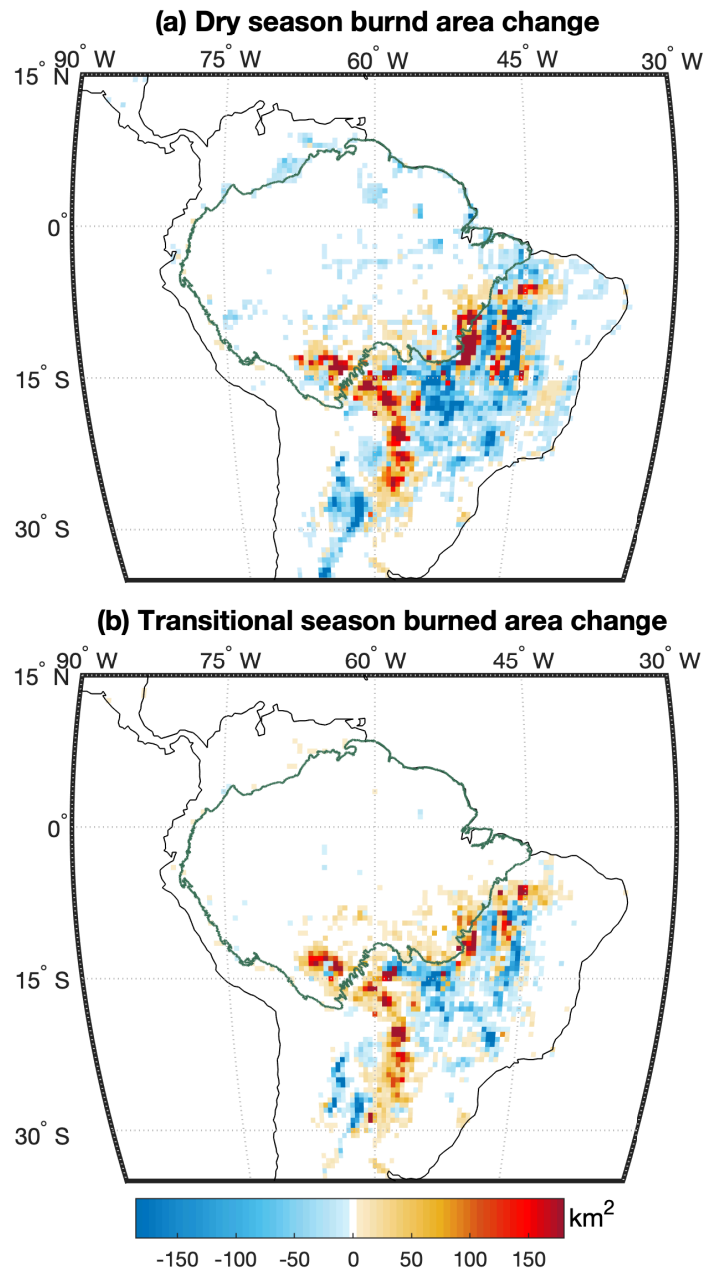
715
716
717
718
719
720

Figure S2: Evolution of drought fraction in entire Am and Aw region. Areal fraction of normal and near-normal drought condition ($-1 < scPDSI < 1$) (a) and areal fraction of slightly to extremely dry drought condition ($scPDSI < -1$) (b) in wet, transition and dry seasons. ** and * denote the significant level of $p < 0.001$ and $p < 0.01$, respectively.



721
722
723
724
725
726
727

Figure S3: Impact of forest loss on latent heat (LE) and surface short-wave net radiation (SSNR). Monthly mean LE change (ΔLE , wm^{-2}) due to accumulated forest loss in Am (a) and Aw (b), and monthly mean SSNR change ($\Delta SSNR$, wm^{-2}) due to accumulated forest loss in Am (c) and Aw (d). The shaded patterns in (a-d) are standard deviation of ΔLE and $\Delta SSNR$ in gridcells with both large forest loss ($F_{loss} > 65\%$) and pristine forest ($F_{loss} < 5\%$) between 2001 and 2017.



729
730
731
732
733

Figure S4: Monthly mean burned area change (km²) during 2001-2017 in relative to 1982-2000. (a) dry season and (b) transition season.